Insights Into an Intriguing Gas Sorption Mechanism in a Polar Metal–Organic Framework with Open-Metal Sites and Narrow Channels

Katherine A. Forrest,[†,§] Tony Pham,[†,§] Keith McLaughlin,[†] Adam Hogan,[†] Brian Space[*,†]
[†]*Department of Chemistry, University of South Florida,*
4202 East Fowler Avenue, CHE205, Tampa, FL 33620-5250, United States
[§]Authors contributed equally
[*]brian.b.space@gmail.com

[Cu(Me-4py-trz-ia)] System Cell

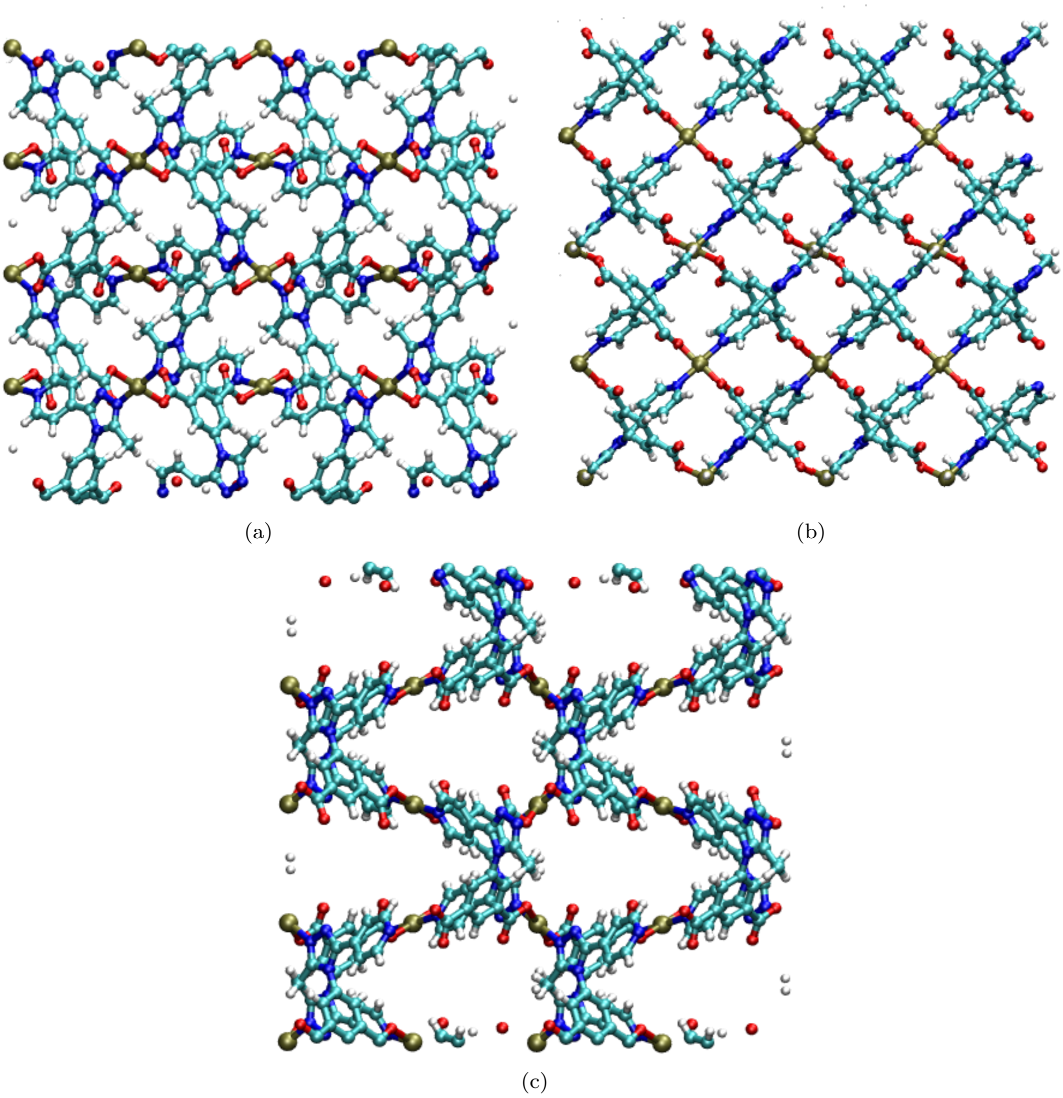
(a)
(b)
(c)

Figure S1. **(a)** The *a* axis view, **(b)** *b* axis view, and **(c)** shifted *c* axis view of the 2 × 2 × 2 unit cell system of [Cu(Me-4py-trz-ia)]. Atom colors: C = cyan, H = white, N = blue, O = red, Cu = tan.

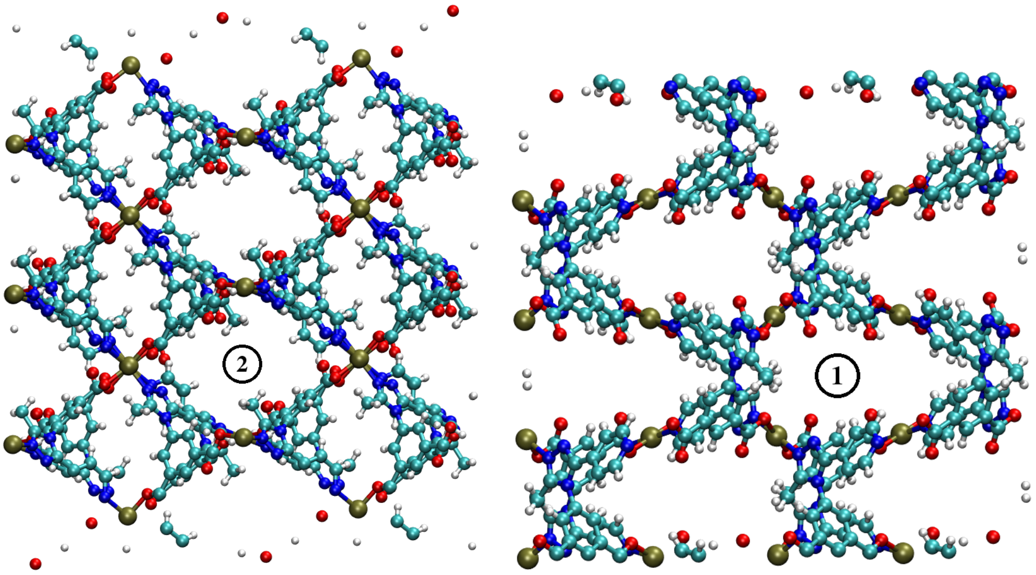

(a) (b)

Figure S2. **(a)** A view of the *ca.* 45° angle between the *a* and *b* axes and **(b)** the shifted *c* axis view of the 2 × 2 × 2 unit cell system of [Cu(Me-4py-trz-ia)]. A singular location of binding sites 1 and 2 are also shown. Atom colors: C = cyan, H = white, N = blue, O = red, Cu = tan.

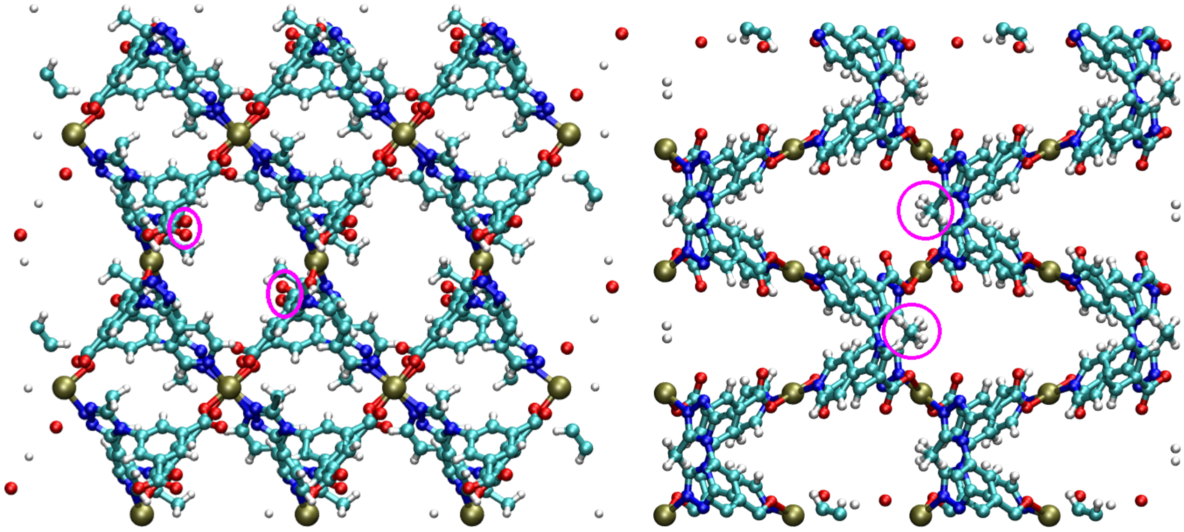

(a) (b)

Figure S3. **(a)** A view of the *ca.* 45° angle between the *a* and *b* axes of the 2 × 2 × 2 unit cell system of [Cu(Me-4py-trz-ia)]. The magenta circles indicate the carboxylate group functionality. The region between the two carboxylate oxygen atoms can only be accessed after prior interaction with the adjacent methyl groups. **(b)** The shifted *c* axis view of the 2 × 2 × 2 unit cell system of [Cu(Me-4py-trz-ia)]. The magenta circles indicate the methyl group functionality. The sorbate molecule must come across the region between the two adjacent methyl groups before it can sorb into the interior of the MOF. Atom colors: C = cyan, H = white, N = blue, O = red, Cu = tan.

Simulation Parameters

Repulsion/dispersion interactions were modeled using the Lennard-Jones 12–6 potential[1] and these parameters (ϵ and σ) were taken from the Optimized Potentials for Liquid Simulations – All Atom (OPLS–AA) force field[2] for all aromatic C and H atoms and the Universal Force Field (UFF)[3] for all other atoms.

The atomic point partial charges for the atoms in [Cu(Me-4py-trz-ia)] were determined from electronic structure calculations on several fragments large enough to mimic the chemical environment of the MOF. Examination of the unit cell for [Cu(Me-4py-trz-ia)] revealed 36 atoms in chemically distinct atomic environments (Figure S4). Indeed, there are two chemically distinct Cu^{2+} ions and each atom on the Me-4py-trz-ia^{2-} linker is chemically distinguishable. This served as the basis for selecting appropriate fragments for charge-fitting calculations. The addition of hydrogen atoms, where appropriate, was required for the chemical termination of fragment boundaries. The fragments that were selected for the charge-fitting calculations for [Cu(Me-4py-trz-ia)] in this study are shown in Figure S5.

All calculations on each fragment were performed using the NWChem *ab initio* simulation software.[4] All light atoms were treated with the 6-31G* basis set, while the LANL2DZ[5–7] effective core potential basis set was used to treat the inner electrons of the Cu^{2+} ions. The former has been shown to produce overpolarized charges that are appropriate for condensed phase simulations.[8] The partial charges were determined through a least-squared fit approach[9,10] to the electrostatic potential surface of each fragment. For each chemically distinct atom, the partial charges were averaged between the fragments. Afterwards, the partial charges were adjusted such that the total charge of the framework was equal to zero. The average partial charges for all chemically distinct atoms for each fragment are shown in Table S1. Note, atoms that are buried or located on the edges of the fragments were not included in the averaging. The final partial charges for each chemically distinct atom for [Cu(Me-4py-trz-ia)] can be found in Table S2.

The atomic point polarizabilities for all light atoms used a set of rigorously parametrized empirical values that were shown to be highly transferable.[11–23] These atoms were assigned the exponential polarizabilities (C = 1.28860 Å^3, H = 0.41380 Å^3, O = 0.85200 Å^3, N = 0.97157 Å^3) and associated damping parameter ($\lambda = 2.1304$) provided by the work of van Duijnen *et al.*[24] An atomic point polarizability value of 2.19630 Å^3 was used to parameterize the Cu^{2+} ions; this parameter was determined in previous work.[17]

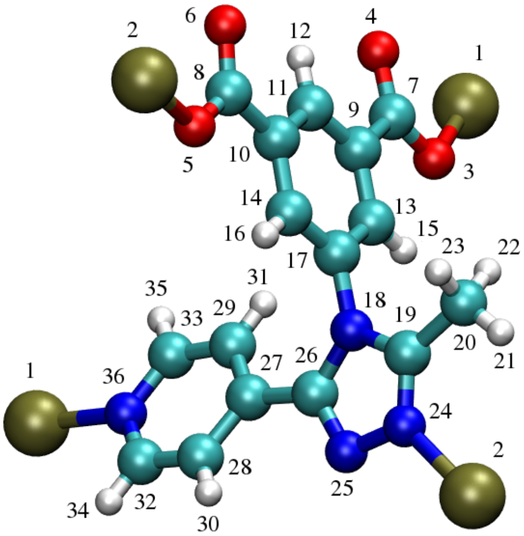

Figure S4. Chemically distinct atoms in [Cu(Me-4py-trz-ia)] as referred to in Tables S1 and S2. Numerical labeling correspond to chemically distinct atoms evaluated. Atom colors: C = cyan, H = white, N = blue, O = red, Cu = tan.

Figure S5. Fragments of [Cu(Me-4py-trz-ia)] that were selected for gas phase charge fitting. Numerical labeling corresponds to chemically distinct atoms evaluated. Atom colors: C = cyan, H = white, O = red, Cu = tan.

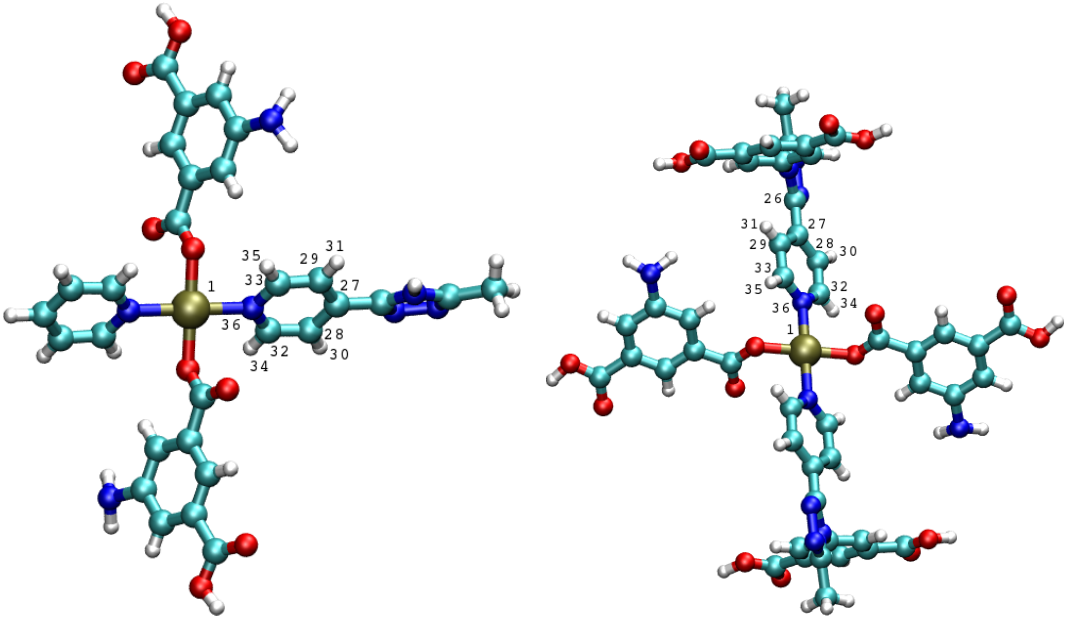

(a)Fragment 1

(b)Fragment 2

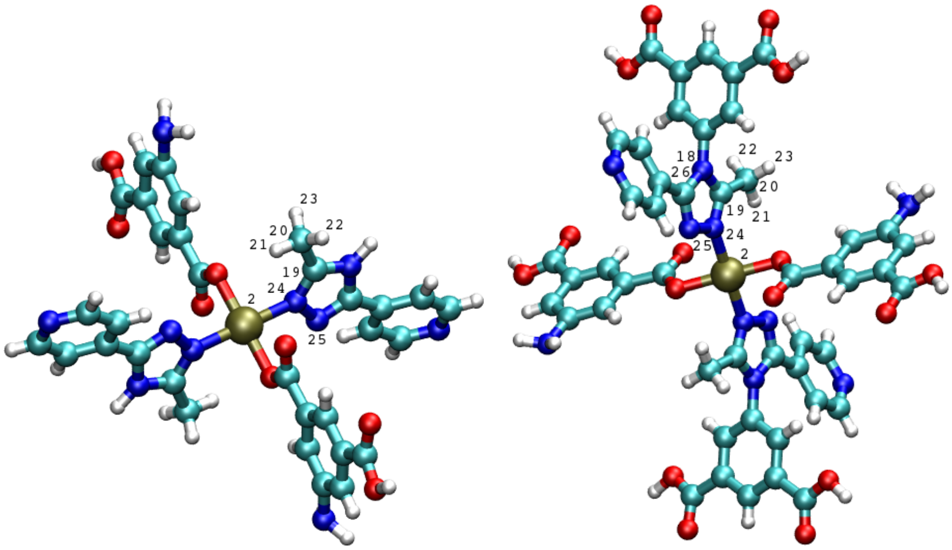

(c)Fragment 3

(d)Fragment 4

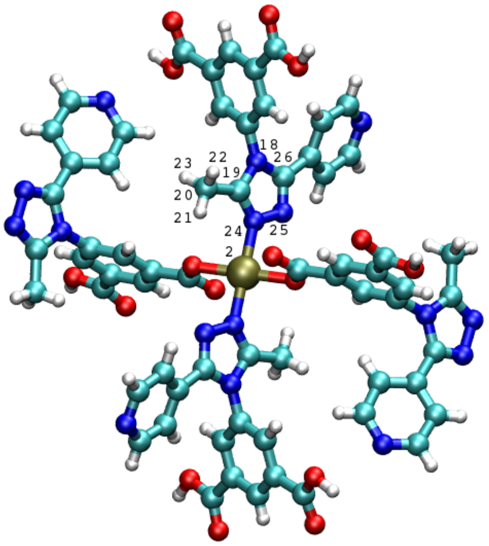

(e)Fragment 5

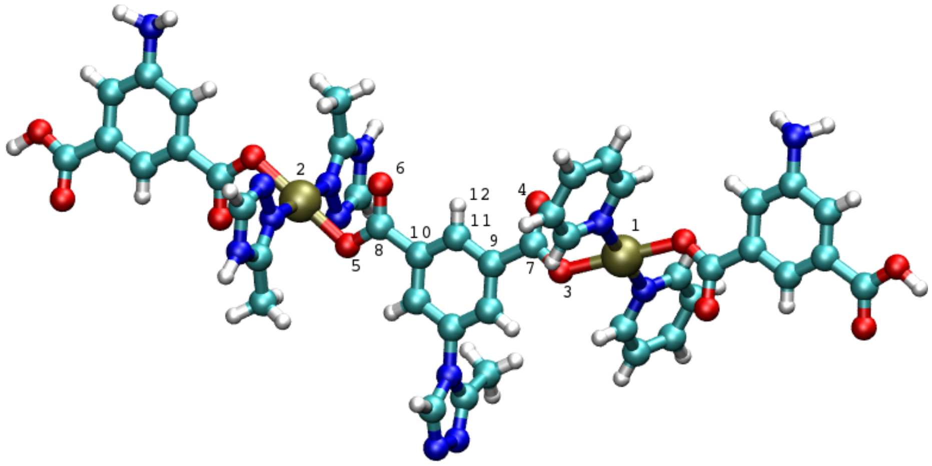

(f)Fragment 6

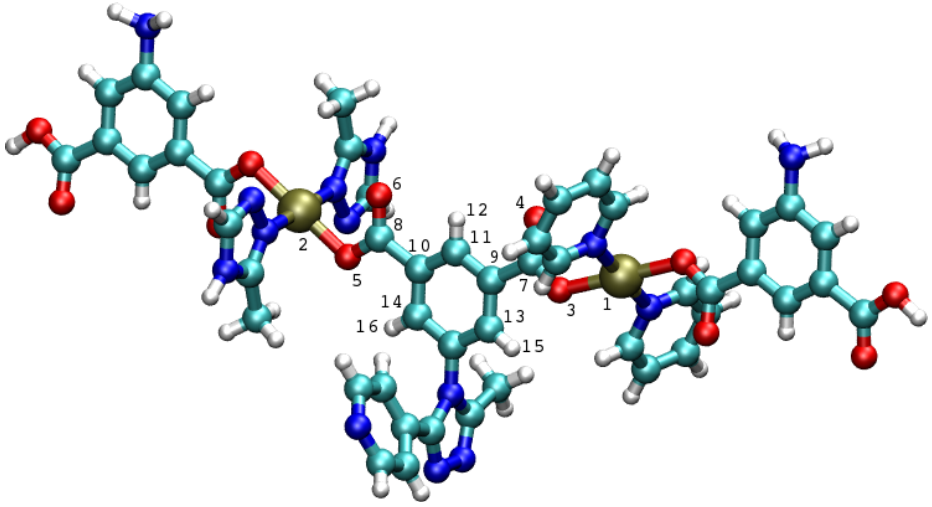

(g)Fragment 7

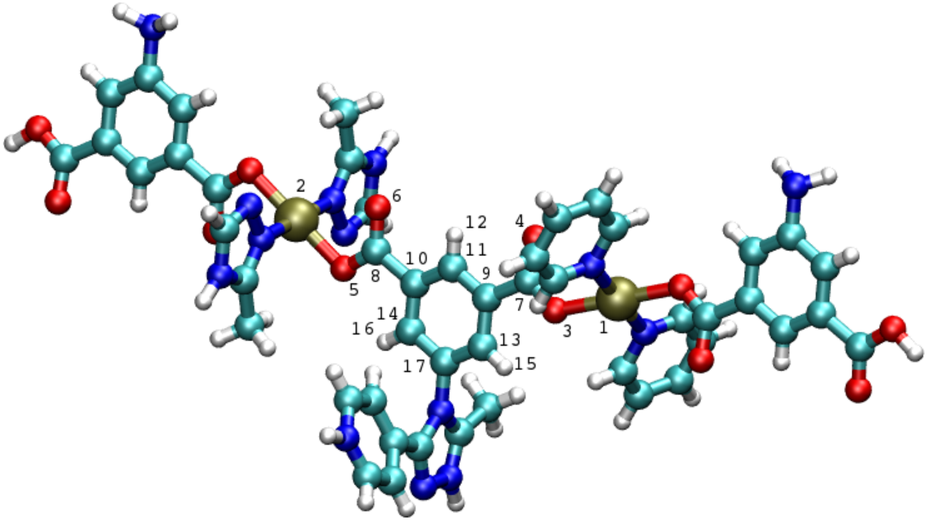

(h)Fragment 8

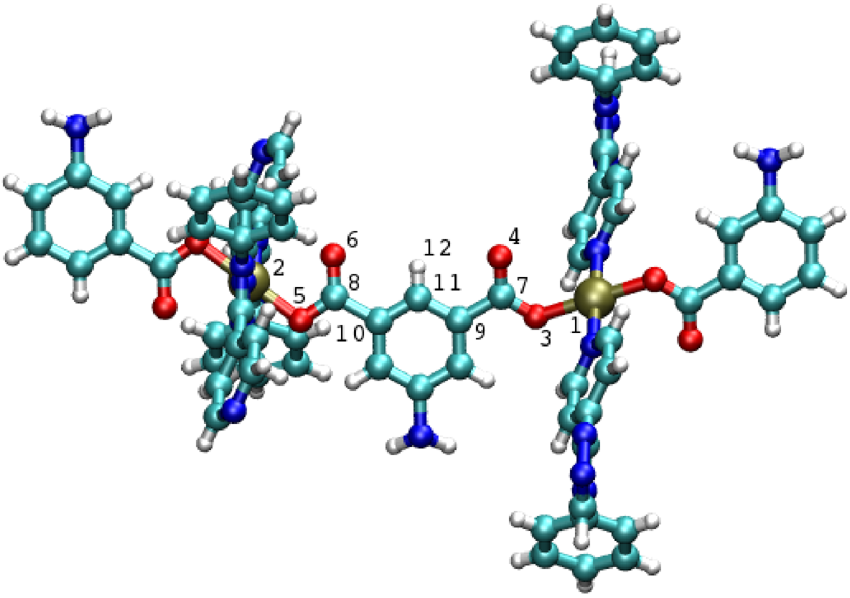

(i)Fragment 9 (Front View)

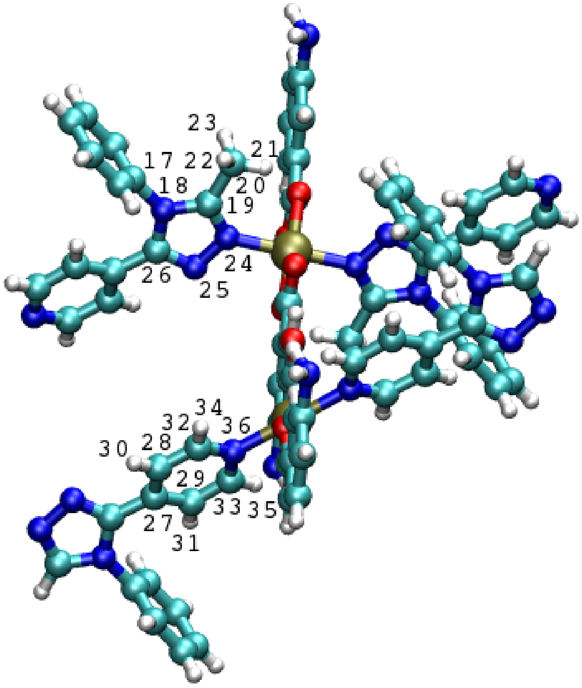

(j)Fragment 9 (Side View)

Atom	Label	Frag 1	Frag 2	Frag 3	Frag 4	Frag 5	Frag 6	Frag 7	Frag 8	Frag 9
Cu	1	0.0808	0.0970	-	-	-	0.0050	-0.0011	0.0165	0.0382
Cu	2	-	-	0.4432	0.4317	0.4716	0.4727	0.4262	0.4311	0.5439
O	3	-	-	-	-	-	-0.5063	-0.5018	-0.5513	-0.5691
O	4	-	-	-	-	-	-0.6381	-0.6232	-0.6003	-0.6471
O	5	-	-	-	-	-	-0.7061	-0.6881	-0.7046	-0.7621
O	6	-	-	-	-	-	-0.7440	-0.7503	-0.7058	-0.7597
C	7	-	-	-	-	-	0.8259	0.8308	0.7877	0.8852
C	8	-	-	-	-	-	0.8363	0.8444	0.8092	0.8926
C	9	-	-	-	-	-	-0.1294	-0.1535	-0.0711	-0.1232
C	10	-	-	-	-	-	-0.0360	-0.0272	0.0426	0.0196
C	11	-	-	-	-	-	-0.1162	-0.1233	-0.1119	-0.1642
H	12	-	-	-	-	-	0.1504	0.1578	0.1690	0.1370
C	13	-	-	-	-	-	-	-0.1858	-0.1966	-
C	14	-	-	-	-	-	-	-0.2192	-0.2494	-
H	15	-	-	-	-	-	-	0.1072	0.1134	-
H	16	-	-	-	-	-	-	0.1620	0.1717	-
C	17	-	0.1517	-	-	-	-	-	0.1659	0.2131
N	18	-	-	-	-0.1737	-0.2045	-	-	-	-0.1111
C	19	-	-	0.3564	0.2797	0.3117	-	-	-	0.3043
C	20	-	-	-0.0996	-0.1444	-0.1458	-	-	-	-0.1167
H	21	-	-	0.1333	0.1662	0.1656	-	-	-	0.1516
H	22	-	-	0.0600	0.0461	0.0421	-	-	-	0.0074
H	23	-	-	0.0335	0.0433	0.0440	-	-	-	0.0420
N	24	-	-	0.0790	0.0691	-0.0047	-	-	-	-0.0064
N	25	-	-	-0.4163	-0.3963	-0.4018	-	-	-	-0.3997
C	26	-	-	-	0.2720	0.2971	-	-	-	0.3269
C	27	-0.0233	-0.0025	-	-	-	-	-	-	-0.0484
C	28	-0.2388	-0.2172	-	-	-	-	-	-	-0.2459
C	29	-0.3074	-0.3374	-	-	-	-	-	-	-0.3087
H	30	0.1360	0.1228	-	-	-	-	-	-	0.1213
H	31	0.1327	0.1520	-	-	-	-	-	-	0.1672
C	32	0.1900	0.1464	-	-	-	-	-	-	0.1633
C	33	0.1190	0.1458	-	-	-	-	-	-	0.1410
H	34	0.1098	0.1107	-	-	-	-	-	-	0.1028
H	35	0.1156	0.1137	-	-	-	-	-	-	0.1152
N	36	-0.0616	-0.0405	-	-	-	-	-	-	0.0002

Table S1. Partial charges for individual fragments of [Cu(Me-4py-trz-ia)] as listed in Figure S5 in units of e^{-}. Label of atoms correspond to Figure S4.

Atom	Label	q (e^-)
Cu	1	0.03940
Cu	2	0.46006
O	3	-0.49370
O	4	-0.58188
O	5	-0.66358
O	6	-0.68652
C	7	0.84563
C	8	0.83240
C	9	-0.00870
C	10	-0.09042
C	11	-0.11746
H	12	0.16478
C	13	-0.21339
C	14	-0.16610
H	15	0.12427
H	16	0.16703
C	17	0.16613
N	18	-0.15129
C	19	0.31298
C	20	-0.11746
H	21	0.15418
H	22	0.04068
H	23	0.03889
N	24	0.03425
N	25	-0.37437
C	26	0.29863
C	27	-0.02293
C	28	-0.21706
C	29	-0.29488
H	30	0.12670
H	31	0.15062
C	32	0.16655
C	33	0.13525
H	34	0.10775
H	35	0.11482
N	36	-0.03153

Table S2. The partial charges (e^-) for the chemically distinct atoms in [Cu(Me-4py-trz-ia)] as used in the simulations. Label of atoms correspond to Figure S4.

Many-Body Polarization

Many-body polarization was explicitly included in the simulations by use of a Thole-Applequist type model.[25–27] An overview of the model used in this work is given here. Consider a static electric field applied to a system containing N atomic sites. The induced dipole, $\vec{\mu}$, at each site i is calculated *via* the following:

$$\vec{\mu}_i = \alpha_i^{\circ} \left(\vec{E}_i^{stat} + \vec{E}_i^{ind} \right) \tag{1}$$

where α° is a scalar atomic point polarizability, $\vec{E}^{stat}$ is the electrostatic field vector due to the atomic point partial charges of the MOF atoms and the sorbate molecules, and $\vec{E}^{ind}$ is the electrostatic field vector due to the atomic induced dipoles. Note, $\vec{E}^{stat}$ is calculated using Wolf summation.[28–30] Rewriting equation 1 in terms of the dipole field tensor, $\hat{\mathbf{T}}_{ij}$, yields the following:

$$\vec{\mu}_i = \alpha_i^{\circ} \left(\vec{E}_i^{stat} - \sum_{j \neq i}^{N} \hat{\mathbf{T}}_{ij} \vec{\mu}_j \right) \tag{2}$$

In this work, the following dipole field tensor is used:

$$\hat{T}_{ij}^{\alpha\beta} \;=\; \nabla^{\alpha} \nabla^{\beta} \left(\frac{s(r)}{r_{ij}} \right) \tag{3}$$

where r_{ij} is the distance between sites i and j and the screening function $s(r) = (\frac{\lambda r}{2} + 1)e^{-\lambda r}$ serves to describe the charge distributions of the interacting dipoles. The damping parameter λ is set to 2.1304, consistent with the work performed by Thole and others, eliminating the short range divergences that occur in the polarization model when dealing with point dipoles (known as the polarization catastrophe).[24,26,31]

Although matrix inversion may be used to find an exact solution to the self-consistent field problem (equation 2), iterative methods can produce a solution in a fraction of the computation time and are extremely stable when Gauss-Seidel relaxation is employed.[30,32] Initially, every induced dipole vector in the system is evaluated as the following:

$$\vec{\mu}_i = \alpha_i^{\circ} \vec{E}_i^{stat} \tag{4}$$

On each subsequent iteration ξ, the dipole field tensor is written as a sum of its lower triangular and strictly upper triangular components $\hat{\mathbf{T}} \equiv \hat{\mathbf{T}}^{\mathbf{L}} + \hat{\mathbf{T}}^{\mathbf{U}}$, and each dipole is updated sequentially *via* forward substitution:

$$\vec{\mu}_i^{\xi} = \alpha_i^{\circ} \left(\vec{E}_i^{stat} - \sum_{i>j} \hat{\mathbf{T}}_{ij}^{L} \vec{\mu}_j^{\xi+1} - \sum_{i<j} \hat{\mathbf{T}}_{ij}^{U} \vec{\mu}_j^{\xi} \right) \tag{5}$$

Finally, the polarization energy for the MOF–sorbate system is calculated by the following based on the work of Palmo and Krimm[33] using the ξ^{th} iteration dipoles and the $(\xi + 1)^{th}$ induced field:

$$U_{pol}^{\xi} = -\frac{1}{2} \sum_i \vec{\mu}_i^{\xi} \cdot \vec{E}_i^{stat} - \frac{1}{2} \sum_i \vec{\mu}_i^{\xi} \cdot \vec{E}_i^{ind,\xi+1} \tag{6}$$

Grand Canonical Monte Carlo

Simulations of H_2 and CO_2 sorption in [Cu(Me-4py-trz-ia)] were performed using grand canonical Monte Carlo (GCMC) on a $2 \times 2 \times 2$ unit cell system of the MOF. This method entails constraining the chemical potential, volume, and temperature to be constant while allowing the particle number and other statistical mechanical quantities to fluctuate.[34] This was achieved by trial insertion and deletion of sorbate molecules based on a random number generator. Periodic boundary conditions were applied in order to approximate an infinitely extended crystal lattice. A spherical cutoff corresponding to half the shortest system cell dimension length was used. The average particle number was calculated by the following expression:[35,36]

$$\langle N \rangle = \frac{1}{\Xi} \sum_{N=0}^{\infty} e^{\beta \mu N} \left\{ \prod_{i=1}^{3N} \int_{-\infty}^{\infty} dx_i \right\} N e^{-\beta U(x_1, \ldots x_{3N})} \tag{7}$$

where Ξ is the grand canonical partition function, β is the inverse temperature (equal to the quantity $1/kT$, where k is the Boltzmann constant and T is the temperature), μ is the chemical potential of the gas reservoir, and U is the total potential energy. The chemical potential for H_2 and CO_2 was determined for a range of temperatures through the BACK[37] and Peng-Robinson equation of state,[38] respectively. The total potential energy of the MOF–sorbate system is calculated by:

$$U = U_{rd} + U_{es} + U_{pol} \tag{8}$$

where U_{rd} is the repulsion/dispersion energy calculated by the Lennard-Jones potential,[1] U_{es} is the electrostatic energy calculated by Ewald summation,[39] and U_{pol} is the polarization energy which is calculated using equation 6.

For the simulations of H_2 sorption at the temperatures considered in this work, quantum mechanical disperion effects were included semiclassically through the fourth-order Feynman-Hibbs correction according to the following equation:[40]

$$U_{FH} = \frac{\beta \hbar^2}{24\mu} \left(U'' + \frac{2}{r} U' \right) + \frac{\beta^2 \hbar^4}{1152 \mu^2} \left(\frac{15}{r^3} U' + \frac{4}{r} U''' + U'''' \right) \tag{9}$$

where $\hbar$ is the reduced Planck's constant and the primes indicate differentiation with respect to pair separation r.

The MOF–sorbate system was also treated with long-range corrections to all terms of the potential due to the finite size of the simulation box. The long-range contribution to the Lennard-Jones potential was calculated by the following based on a previously reported method:[41]

$$U_{LJ}^{LRC} = \frac{16\pi}{3V} \sum_{i=0}^{N-1} \sum_{j=0}^{N-1} \epsilon_{ij} \left(\frac{\sigma_{ij}^9}{3R_c^9} - \frac{\sigma_{ij}^3}{R_c^3} \right) \tag{10}$$

where ϵ_{ij} and σ_{ij} are Lorentz-Berthelot mixed Lennard-Jones parameters, V is the volume of the simulation box, and R_C is the cut-off distance, which is set to one-half the shortest simulation box length.

Long-range electrostatic interactions were handled by performing full Ewald summation. The long-range correction to the polarization energy was performed by replacing the static electric field with the shifted-field formula according to Wolf *et al.*,[28,29] which is the following:

$$\vec{E}_i^{shift} = \sum_{j}^{N-1} q_j \left(\frac{1}{r_{ij}^2} - \frac{1}{R_c^2} \right) \hat{r} \tag{11}$$

where q is the atomic point partial charge and $\hat{r}$ is the radial unit vector.

In GCMC simulation, the excess sorbate uptake, defined as the amount sorbed in the pore volume in excess of the bulk gas capacity in the same free space,[42] was determined from a calculation that utilized an experimental pore volume value[43] of 0.586 cm^3 g^{-1} and bulk gas densities *via* the following expression:

$$R_{ex} = 1000 \frac{m(\langle N \rangle - V_p \rho_b)}{M} \tag{12}$$

where V_p is the pore volume, ρ_b is the bulk gas density, m is the molar mass of the sorbate, and M is the molar mass of the MOF.

The theoretical isosteric heats of adsorption, Q_{st}, were calculated based on the fluctuations of the particle number and total potential energy in the MOF–sorbate system through the following expression:[44]

$$Q_{st} = -\frac{\langle NU\rangle - \langle N\rangle\langle U\rangle}{\langle N^2\rangle - \langle N\rangle^2} + kT \tag{13}$$

For all state points considered, the simulations consisted of 2×10^6 Monte Carlo steps to guarantee equilibration, followed by an additional 2×10^6 steps to sample the desired thermodynamic properties. The simulations utilized a correlation time of 1×10^4 steps in order to guarantee uncorrelated configurations. All simulations were performed using the Massively Parallel Monte Carlo (MPMC) code,[45] which is currently available for download on Google Code.

Prediction of Pore Volume Through Helium Adsorption

The theoretical pore volume of [Cu(Me-4py-trz-ia)] was calculated using a previously reported molecular simulation prcoedure.[46] The relationship between the absolute amount of sorbed molecules, N_{abs}, and the amount of sorbed molecules in excess of the number of molecules that would occupy the free pore volume at bulk gas conditions, N_{ex}, is represented by the following equation:[42]

$$N_{ex} = N_{abs} - V_p \rho_b \tag{14}$$

where V_p is the pore volume and ρ_b is the bulk phase density. For helium at ambient temperature, N_{ex} is equal to 0 because it is a non-adsorbing (or weakly adsorbing) gas, and thus, equation 14 becomes the following:

$$V_p = \frac{N_{abs}}{\rho_b} \tag{15}$$

At low pressures, helium is assumed to exhibit ideal behavior and this yields equation 15 as:

$$V_p = \frac{N_{abs} kT}{P} \tag{16}$$

where k is the Boltzmann constant, T is the temperature, and P is the pressure.
The adsorption second virial coefficient from experiment and simulation is calculated by:

$$B_{ex} = kT \lim_{P \to 0} \left(\frac{dN_{ex}}{dP} \right) \tag{17}$$

and

$$B_{abs} = kT \lim_{P \to 0} \left(\frac{dN_{abs}}{dP} \right) \tag{18}$$

Combining equations 14, 17, and 18 gives

$$B_{ex} = B_{abs} - V_p \tag{19}$$

For helium, both N_{ex} and B_{ex} are equal to zero, so equation 19 becomes:

$$V_p = B_{abs} \approx kTm \tag{20}$$

where m is the slope of the nearly linear helium adsorption isotherm as P approaches zero. Thus, GCMC simulations of helium sorption were performed in [Cu(Me-4py-trz-ia)] at 298 K and pressures up to 50.0 atm using a previously reported helium model (ϵ = 10.22 K; σ = 2.28 Å).[47] The helium sorption isotherm in [Cu(Me-4py-trz-ia)] is shown in Figure S6. The slope (in units of cm^3 g^{-1} atm^{-1}) was determined from linear fitting of the isotherm (R^2 = 0.999) and it was used in equation 20 for the calculation of the theoretical pore volume. In this work, the pore volume was calculated to be 0.591 cm^3 g^{-1}, which is very close to the experimental value of 0.586 cm^3 g^{-1}.

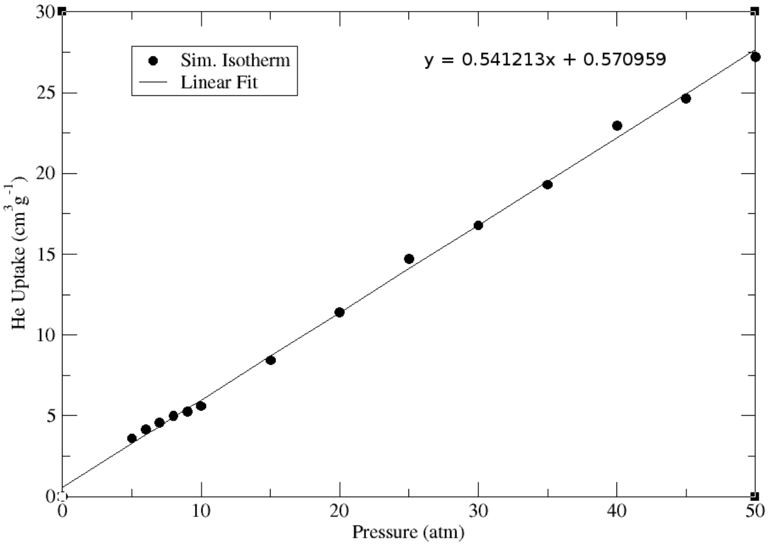

Figure S6. The simulated He sorption isotherm at 298 K and up to 50.0 atm for [Cu(Me-4py-trz-ia)]. The linear fitting of the sorption isotherm is also shown.

Sorbate Potentials

The H_2 potential employed in this work is a five–site polarizable model that includes partial charges and atomic point polarizabilities on the center-of-mass position and the location of the H atoms (H–H distance is 0.742 Å). These quantities represent the molecular quadrupole and polarizability tensor of H_2, respectively. In addition, this model contains Lennard-Jones parameters that are localized on the center-of-mass site and two phantom sites that extend 0.363 Å from the center-of-mass site along the C_∞ axis. This model is known to reproduce high density hydrogen in the bulk environment and is capable of describing the proper sorption behavior in highly charged/polar MOFs.[48]

The CO_2 potential used herein is a five–site polarizable model that contains partial charges and atomic point polarizabilities localized on the atomic locations of the carbon and oxygen atoms (C–O distance is 1.162 Å). Although the point polarizability values are representative of the polarizability tensor for CO_2, the partial charges slightly overestimate the molecular quadrupole for the compound; the latter finding could attributed to the limitation of the potential form. Further, there are Lennard-Jones parameters that are located on the carbon atom and the off-site positions that extend 1.114 Å away from the carbon atom. This model is capable of reproducing bulk CO_2 data and describing sorption in MOFs where induced dipole effects are critical.[49] The parameters for both H_2 and CO_2 models can be found in Table S3.

Model	Atomic Site	ϵ(K)	σ(Å)	q (e^-)	α°(Å^3)
H_2	COM	12.76532	3.15528	-0.74640	0.69380
	H	0.00000	0.00000	0.37320	0.00044
	OS	2.16726	2.37031	0.00000	0.00000
CO_2	C	19.61757	3.30366	0.77134	1.22810
	O	0.00000	0.00000	-0.38567	0.73950
	OS	46.47457	2.99429	0.00000	0.00000

Table S3. Parameters used to characterize the polarizable H_2 and CO_2 potentials used in this work. COM refers to the center-of-mass position and OS refers to the off-site positions.

H_2 Sorption Results

Figure S7 shows that the simulated low-pressure (up to 100 kPa) excess H_2 sorption isotherms in [Cu(Me-4py-trz-ia)] are slightly higher than experiment at 77 K and 87 K at all pressures considered, whereas it is in rather good agreement with experiment at 97 K. All experimental data points in this figure were estimated from reference 43. However, at all state points considered, the simulated uptakes are in very good agreement with the corresponding experimental uptakes to within joint uncertainties. The simulated H_2 sorption isotherm in [Cu(Me-4py-trz-ia)] at 77 K and higher pressures (up to 3.0 MPa) is also in good agreement with experiment (data points estimated from reference 43) for the pressure range considered (Figure S8). The maximum calculated excess H_2 uptake was approximately 20.0 mmol g^{-1}, which is consistent with experimental measurements.

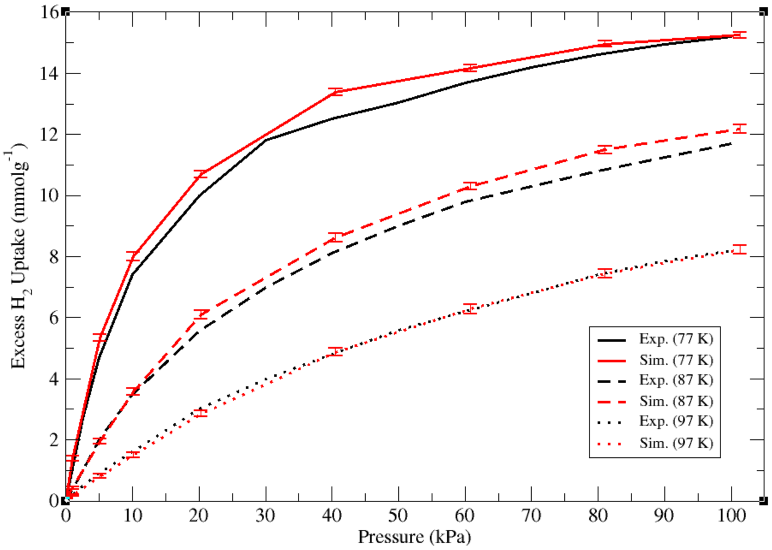

Figure S7. Low-pressure (up to 1.0 atm) excess H_2 sorption isotherms in [Cu(Me-4py-trz-ia)] at 77 K (solid), 87 K (dashed), and 97 K (dotted) for experiment (black) and simulation (red).

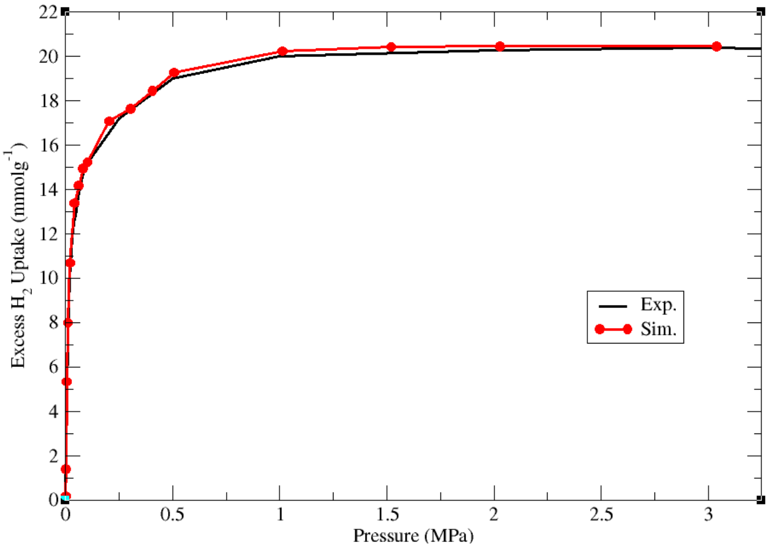

Figure S8. High-pressure (up to 30.0 atm) excess H_2 sorption isotherms in [Cu(Me-4py-trz-ia)] at 77 K for experiment (black) and simulation (red). Note, the error bars at each state point for the simulated plot are small, especially at higher pressures, and thus, have been omitted for clarity.

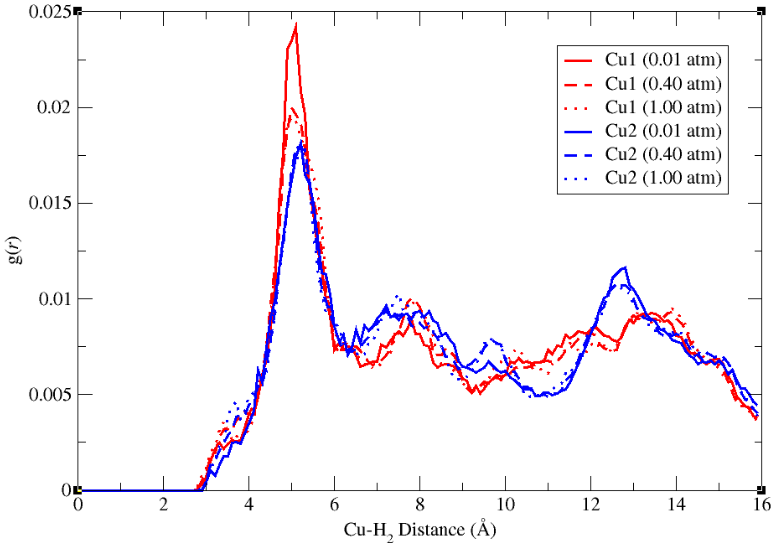

Figure S9. Radial distribution functions, g(r), for H_2 molecules about the Cu1 ions (atom label 1 in Figure S4) (red) and the Cu2 ions (atom label 2 in Figure S4) (blue) in [Cu(Me-4py-trz-ia)] at 77 K and pressures of 0.01 atm (solid), 0.40 atm (dashed), and 1.0 atm (dotted).

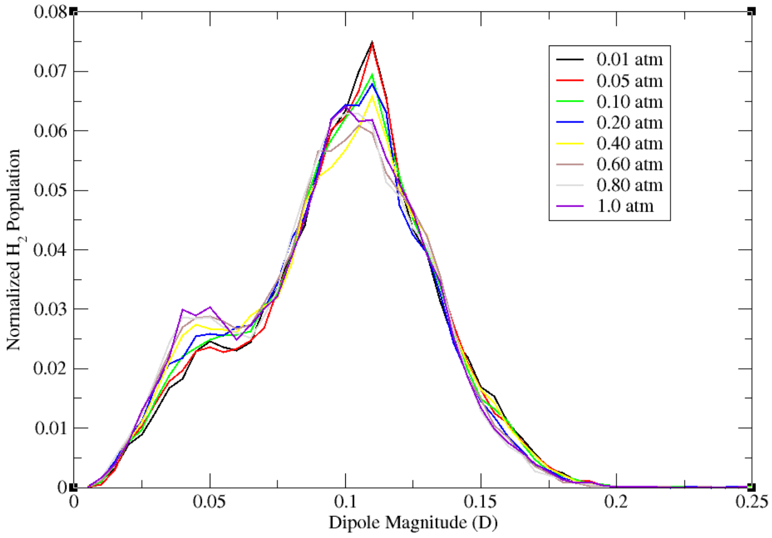

Figure S10. Normalized H_2 dipole distribution at 77 K and various pressures in [Cu(Me-4py-trz-ia)]. The region from 0.065 to 0.20 Debye corresponds to sorption to site 1. The region from 0.00 to 0.065 Debye corresponds to sorption to site 2.

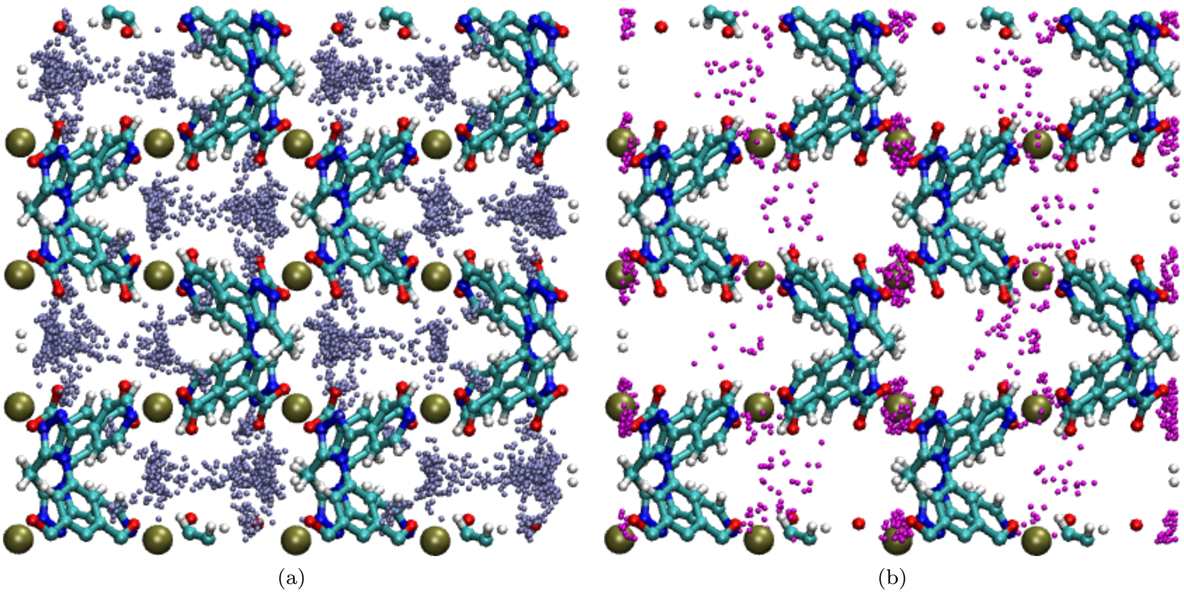
(a) (b)

Figure S11. The shifted *c* axis view of the 2 × 2 × 2 unit cell system of [Cu(Me-4py-trz-ia)] showing the sites of H_2 sorption as a function of induced dipole magnitude according to Figure S10: **(a)** 0.065 to 0.20 Debye; **(b)** 0.00 to 0.065 Debye. Atom colors: C = cyan, H = white, N = blue, O = red, Cu = tan.

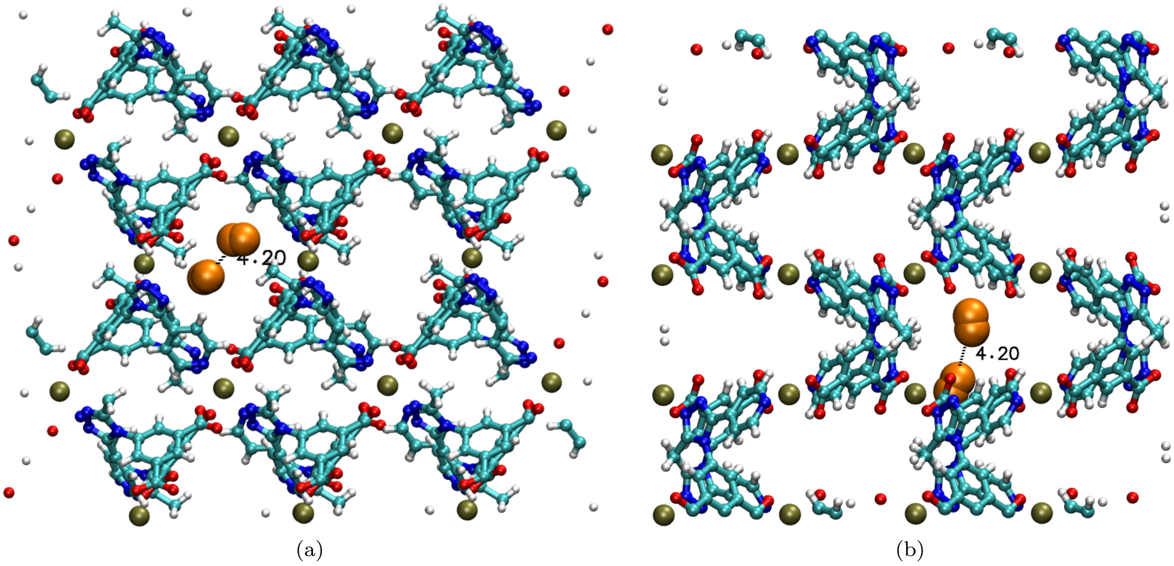

(a) (b)

Figure S12. **(a)** A view of the *ca.* 45° angle between the *a* and *b* axes and **(b)** the shifted *c* axis view of the 2 × 2 × 2 unit cell system of [Cu(Me-4py-trz-ia)] showing the positions of the sorbed H_2 molecules about sites 1 and 2 from simulated annealing. The sorbate molecules are shown in orange. The distance between the two center-of-mass sites is 4.20 Å. Atom colors: C = cyan, H = white, N = blue, O = red, Cu = tan.

CO_2 Sorption Results

All simulated excess CO_2 sorption isotherms in comparison with the corresponding experimental data (produced by using the parameters from reference 43) in [Cu(Me-4py-trz-ia)] are shown in Figure S13. Figure S13(a) shows that the simulated high pressure (up to 4.0 MPa) CO_2 sorption isotherm at 273 K are in excellent agreement with the experimental isotherm at all pressures considered at this temperature. It can be observed that the experimental isotherm reaches CO_2 saturation at approximately 1.0 MPa at this temperature with a value of about 12.0 mmol g^{-1}. The simulated CO_2 sorption isotherm also saturates at approximately 12.0 mmol g^{-1}, as demonstrated by the excellent agreement between experiment and simulation for all pressures considered at 273 K as shown in Figure S13(a). The simulated CO_2 sorption isotherm at 298 K is in excellent agreement with experiment at pressures up to 0.10 MPa (Figure S13(b)). However, at pressures of 0.20 MPa and above, the simulated uptakes are notably higher than experiment at this temperature. It can be observed in Figure S13(c) that, at 323 K, the simulated sorption isotherm undersorbs experiment at low pressures (up to 0.50 MPa) and oversorbs experiment at higher pressures (1.0 MPa and above). In general, the simulated CO_2 uptakes agree with the corresponding experimental measurements to within joint uncertainties at all state points considered and the conclusions presented in the manuscript are not materially affected by the differences.

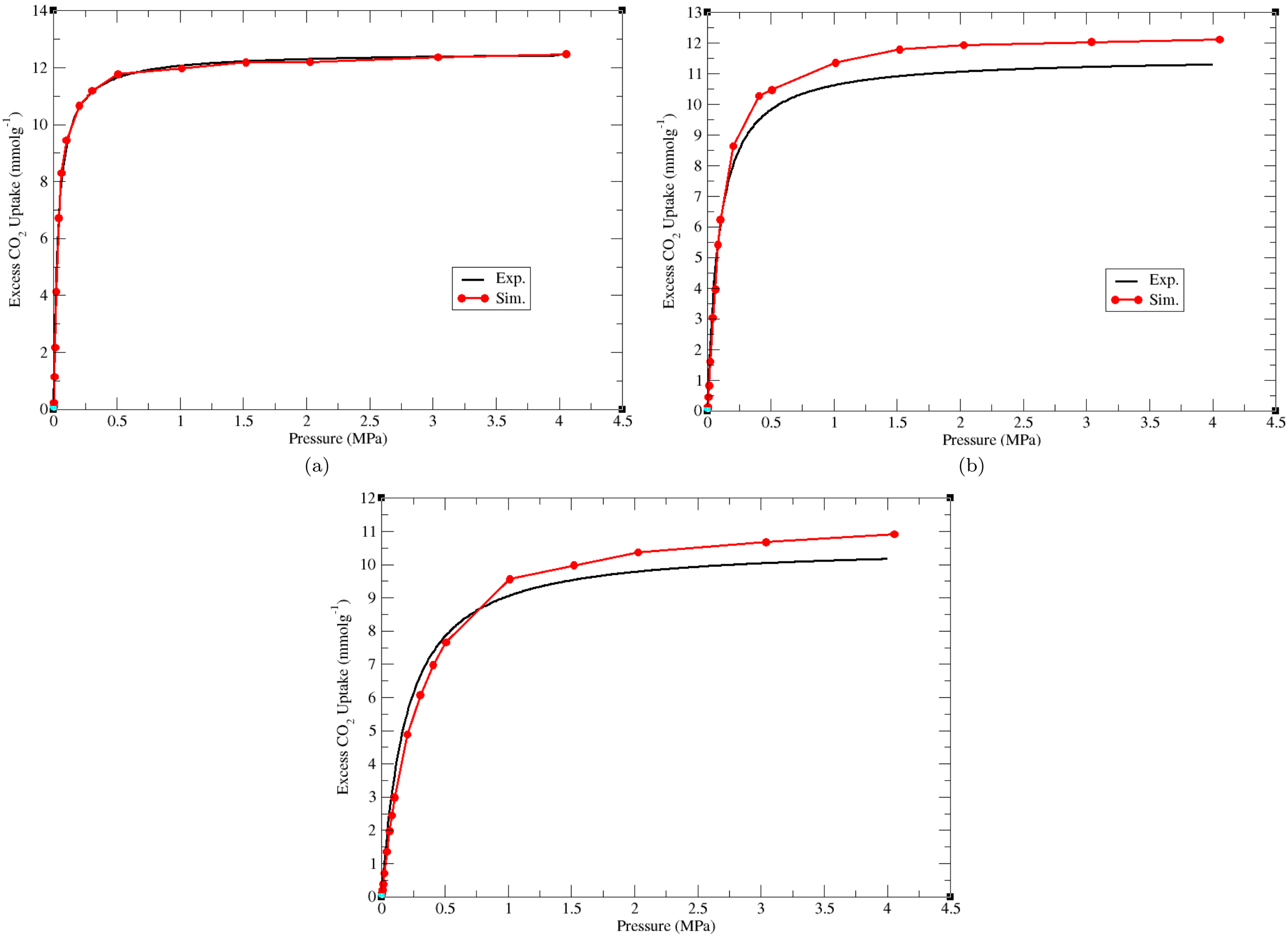

(a)

(b)

(c)

Figure S13. High-pressure (up to 40.0 atm) excess CO_2 sorption isotherms in [Cu(Me-4py-trz-ia)] at **(a)** 273 K, **(b)** 298 K, and **(c)** 323 K for experiment (black) and simulation (red). Note, the error bars at each state point for the simulated plots are small, especially at higher pressures, and thus, have been omitted for clarity.

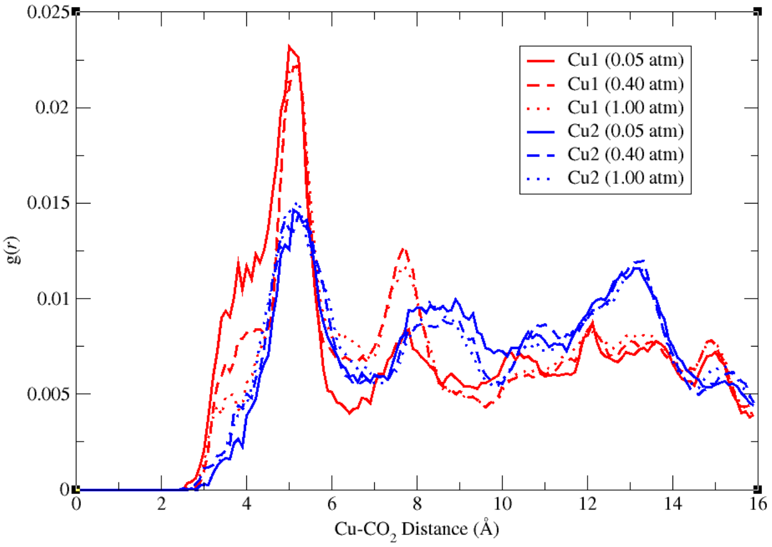

Figure S14. Radial distribution functions, g(r), for CO_2 molecules about the Cu1 ions (atom label 1 in Figure S4) (red) and Cu2 ions (atom label 2 in Figure S4) (blue) in [Cu(Me-4py-trz-ia)] at 273 K and pressures of 0.05 atm (solid), 0.40 atm (dashed), and 1.0 atm (dotted).

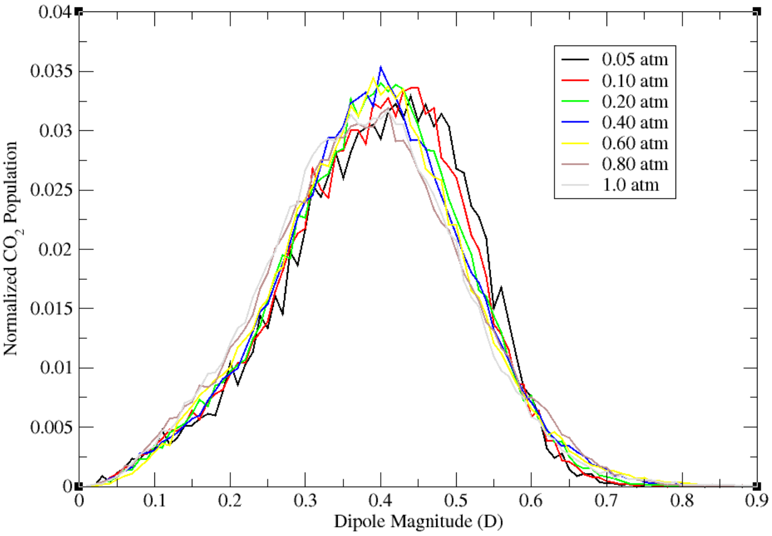

Figure S15. Normalized CO_2 dipole distribution at 273 K and various pressures in [Cu(Me-4py-trz-ia)]. The region from 0.30 to 0.80 Debye corresponds to sorption to site 1. The region from 0.00 to 0.12 Debye corresponds to sorption to site 2. The region from 0.12 to 0.30 Debye corresponds to sorption to both sites 1 and 2.

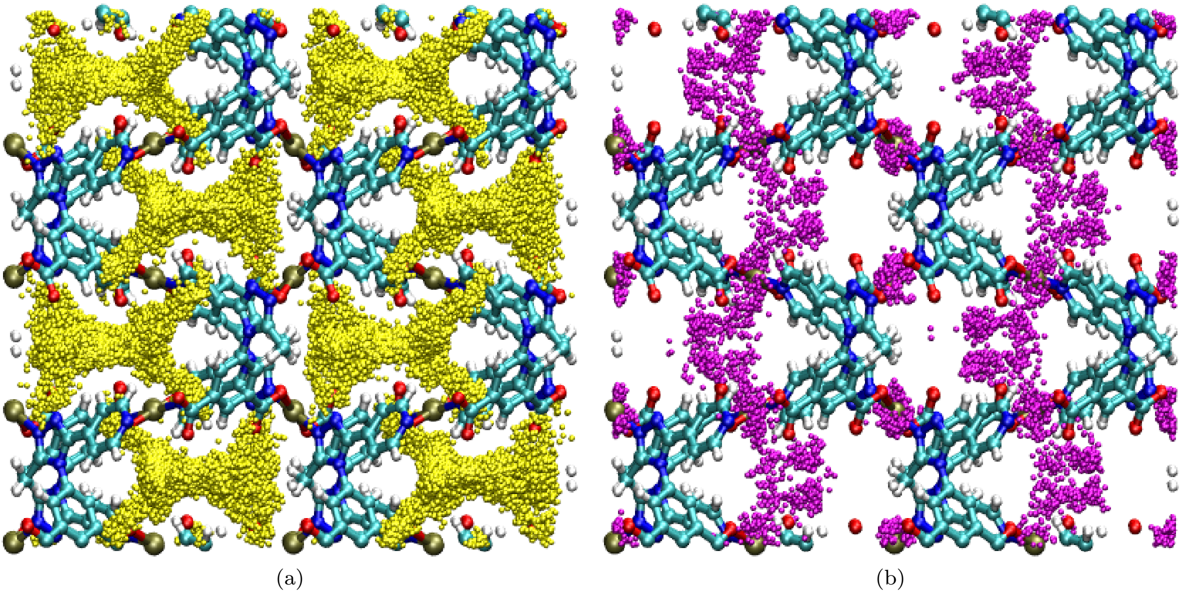
(a) (b)

Figure S16. The shifted *c* axis view of the 2 × 2 × 2 unit cell system of [Cu(Me-4py-trz-ia)] showing the sites of CO_2 sorption as a function of induced dipole magnitude according to Figure S15: **(a)** 0.30 to 0.80 Debye; **(b)** 0.00 to 0.12 Debye. Atom colors: C = cyan, H = white, N = blue, O = red, Cu = tan.

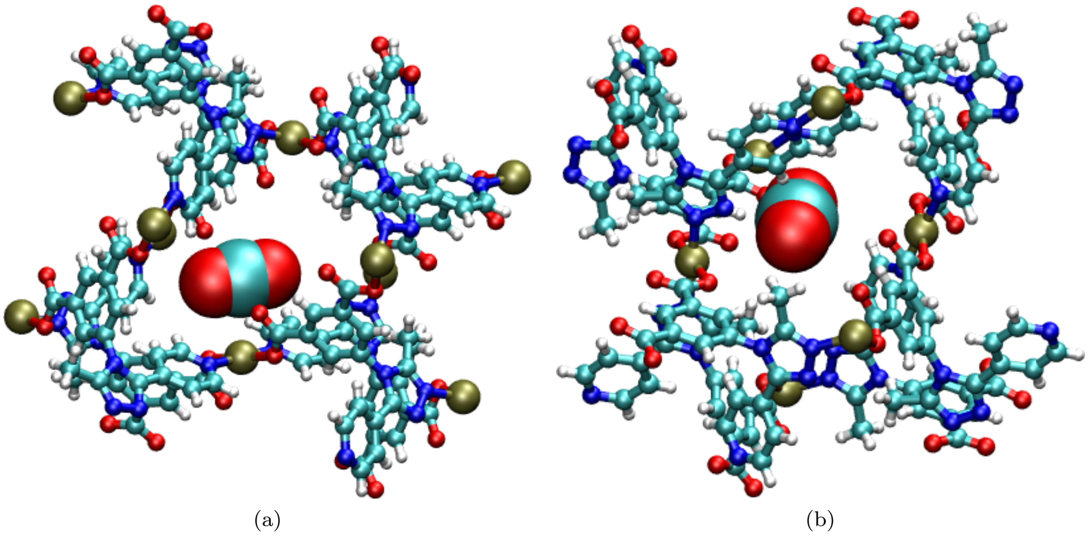
(a) (b)

Figure S17. Molecular illustration of a sorbed CO_2 molecule about **(a)** site 1 and **(b)** site 2 in [Cu(Me-4py-trz-ia)] as determined from simulation. Note, orientational constraints are not imposed on the CO_2 molecule at the binding sites. Atom colors: C = cyan, H = white, N = blue, O = red, Cu = tan.

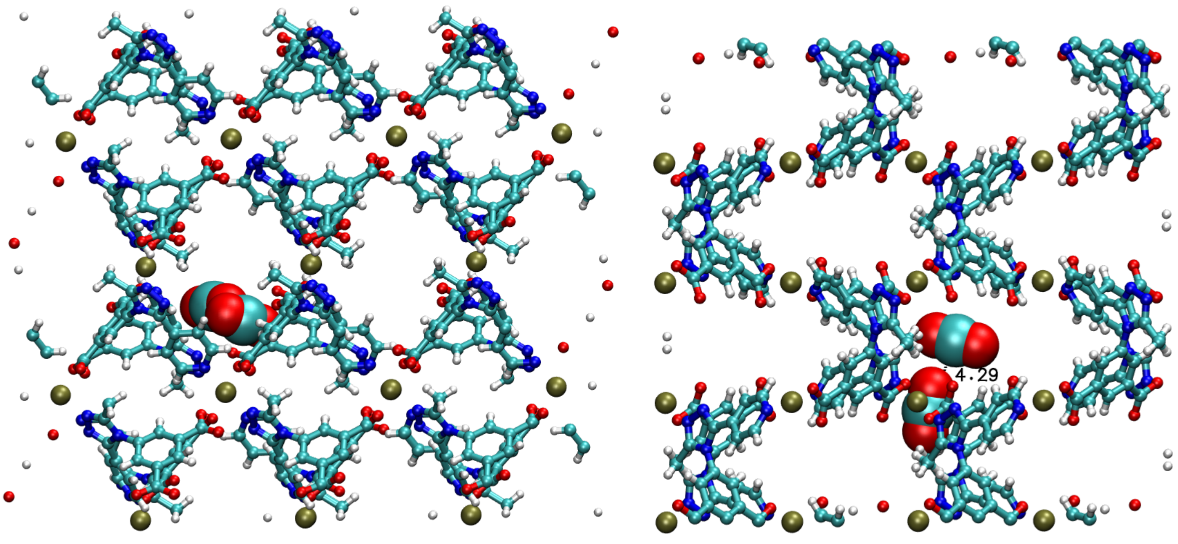

(a) (b)

Figure S18. **(a)** A view of the *ca.* 45° angle between the *a* and *b* axes and **(b)** the shifted *c* axis view of the 2 × 2 × 2 unit cell system of [Cu(Me-4py-trz-ia)] showing the positions of the sorbed CO_2 molecules about sites 1 and 2 from simulated annealing. The distance between the two CO_2 carbon atoms is 4.29 Å. Atom colors: C = cyan, H = white, N = blue, O = red, Cu = tan.

Molecular Dynamics Simulations

Molecular dynamics (MD) simulations were performed in [Cu(Me-4py-trz-ia)] using an in-house modification of the Large-scale Atomic/Molecular Massively Parallel Simulator (LAMMPS) code[50] to include many-body polarization.[51] The same MOF parameters and sorbate models that were used in the Monte Carlo simulations were used for the MD simulations, including assuming the framework is rigid. The H_2 sorption simulation was performed with microcanonical (NVE) integration and a timestep of 2 fs. A single hydrogen molecule was simulated at a location between two adjacent methyl groups (site 2); this was obtained from the GCMC simulations. The hydrogen molecule was given a velocity large enough to overcome the potential energy well between the two methyl groups and explore the rest of the framework, including traveling to the region between two adjacent carboxylate oxygen atoms (site 1). A portion of the hydrogen molecule's trajectory was extracted around the time of a transition from site 2 to site 1 and single point energies at each timestep were calculated using the MPMC code.[45] The CO_2 sorption simulation was performed in a similar manner, with the exception that Nosé-Hoover style canonical (NVT) integration was used with the temperature set at 200 K and with a temperature damping time of 100 timesteps.

A plot of single-point energies as the H_2 molecule travels from site 2 to site 1 in [Cu(Me-4py-trz-ia)] is shown in Figure S19(a). The fluctuations in energy at the beginning can be attributed to librational effects from the starting position (site 2). Nevertheless, as the H_2 molecule escapes site 2 and makes its way over to site 1, it must overcome a barrier that is approximately 0.80 kJ mol^{-1} in energy. This is a rather low value as it suggests that the hydrogen molecules can easily jump from site 2 to site 1 in this MOF at 77 K. A plot of similar type can be seen for CO_2 sorption in Figure S19(b). It was observed that the barrier height for the transition from site 2 to site 1 (measuring from the well of site 2 to the highest energy conformation) is approximately 10.5 kJ mol^{-1}, which is significant, but is clearly overcome in filling the sites under the conditions considered. Note that in the case of CO_2, the transition between site 2 to site 1 is characterized by several energy peaks with shallow minima in between them. This is because the bulky methyl functionality hinders a smooth transition from site 2 to site 1 for the large CO_2 molecule.

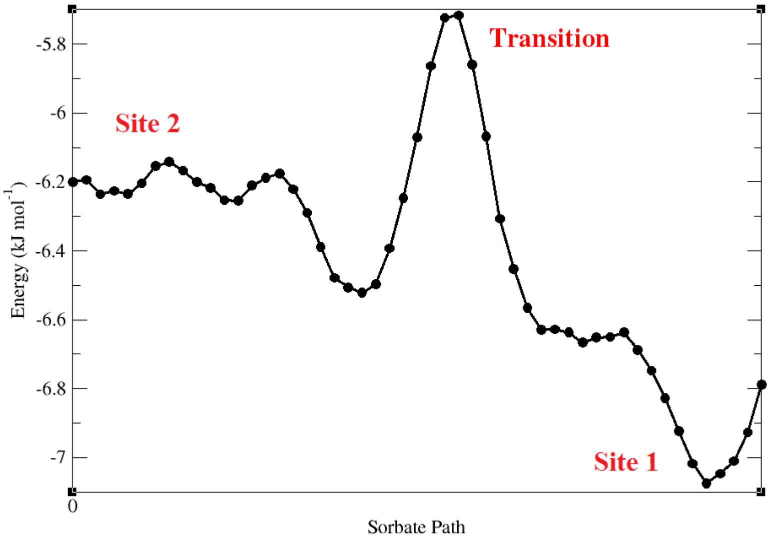

(a)

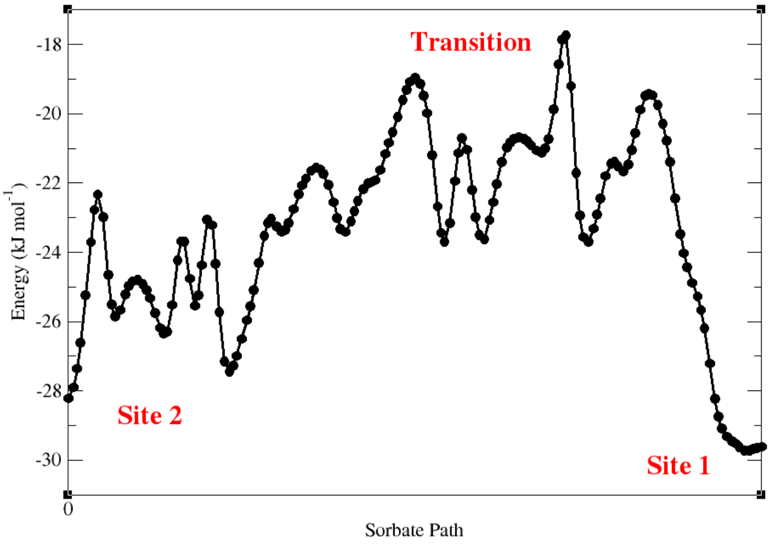

(b)

Figure S19. A plot of single-point energies as the sorbate molecule travels from site 2 to site 1 in [Cu(Me-4py-trz-ia)] as determined with the aid of molecular dynamics simulations: **(a)** H_2; **(b)** CO_2.

[1] Jones, J. On the determination of molecular fields. II. From the equation of state of a gas. *Proceedings of the Royal Society of London. Series A, Containing Papers of a Mathematical and Physical Character* **1924**, *106*, 463–477.

[2] Jorgensen, W. L.; Maxwell, D. S.; Tirado-Rives, J. Development and Testing of the OPLS All–Atom Force Field on Conformational Energetics and Properties of Organic Liquids. *Journal of the American Chemical Society* **1996**, *118*, 11225–11236.

[3] Rappé, A. K.; Casewit, C. J.; Colwell, K. S.; Goddard, W. A.; Skiff, W. M. UFF, a full periodic table force field for molecular mechanics and molecular dynamics simulations. *Journal of the American Chemical Society* **1992**, *114*, 10024–10035.

[4] Valiev, M.; Bylaska, E.; Govind, N.; Kowalski, K.; Straatsma, T.; Dam, H. V.; Wang, D.; Nieplocha, J.; Apra, E.; Windus, T.; de Jong, W. NWChem: A comprehensive and scalable open-source solution for large scale molecular simulations. *Computer Physics Communications* **2010**, *181*, 1477 – 1489.

[5] Stevens, W. J.; Basch, H.; Krauss, M. Compact effective potentials and efficient sharedexponent basis sets for the first and secondrow atoms. *Journal of Chemical Physics* **1984**, *81*, 6026.

[6] Hay, P. J.; Wadt, W. R. Ab initio effective core potentials for molecular calculations. Potentials for the transition metal atoms Sc to Hg. *Journal of Chemical Physics* **1985**, *82*, 270.

[7] LaJohn, L. A.; Christiansen, P. A.; Ross, R. B.; Atashroo, T.; Ermler, W. C. Ab initio relativistic effective potentials with spinorbit operators. III. Rb through Xe. *Journal of Chemical Physics* **1987**, *87*, 2812.

[8] Cornell, W. D.; Cieplak, P.; Bayly, C. I.; Gould, I. R.; Merz, K. M.; Ferguson, D. M.; Spellmeyer, D. C.; Fox, T.; Caldwell, J. W.; Kollman, P. A. A Second Generation Force Field for the Simulation of Proteins, Nucleic Acids, and Organic Molecules. *Journal of the American Chemical Society* **1995**, *117*, 5179–5197.

[9] Chirlian, L. E.; Francl, M. M. Atomic charges derived from electrostatic potentials: A detailed study. *Journal of Computational Chemistry* **1987**, *8*, 894–905.

[10] Breneman, C. M.; Wiberg, K. B. Determining atom-centered monopoles from molecular electrostatic potentials. The need for high sampling density in formamide conformational analysis. *Journal of Computational Chemistry* **1990**, *11*, 361–373.

[11] DeVane, R.; Space, B.; Perry, A.; Neipert, C.; Ridley, C.; Keyes, T. A time correlation function theory of two-dimensional infrared spectroscopy with applications to liquid water. *Journal of Chemical Physics* **2004**, *121*, 3688–3701.

[12] Perry, A.; Neipert, C.; Space, B.; Moore, P. B. Theoretical Modeling of Interface Specific Vibrational Spectroscopy: Methods and Applications to Aqueous Interfaces. *Chemical Reviews* **2006**, *106*, 1234–1258, PMID: 16608179.

[13] Belof, J. L.; Stern, A. C.; Eddaoudi, M.; Space, B. On the Mechanism of Hydrogen Storage in a Metal–Organic Framework Material. *Journal of the American Chemical Society* **2007**, *129*, 15202–15210, PMID: 17999501.

[14] Stern, A. C.; Belof, J. L.; Eddaoudi, M.; Space, B. Understanding hydrogen sorption in a polar metal–organic framework with constricted channels. *Journal of Chemical Physics* **2012**, *136*, 034705.

[15] Cirera, J.; Sung, J. C.; Howland, P. B.; Paesani, F. The effects of electronic polarization on water adsorption in metal–organic frameworks: H_2O in MIL-53(Cr). *Journal of Chemical Physics* **2012**, *137*, 054704.

[16] Paesani, F. Water in metal–organic frameworks: structure and diffusion of H_2O in MIL-53(Cr) from quantum simulations. *Molecular Simulation* **2012**, *38*, 631641.

[17] Forrest, K. A.; Pham, T.; McLaughlin, K.; Belof, J. L.; Stern, A. C.; Zaworotko, M. J.; Space, B. Simulation of the Mechanism of Gas Sorption in a Metal–Organic Framework with Open Metal Sites: Molecular Hydrogen in PCN-61. *The Journal of Physical Chemistry C* **2012**, *116*, 15538–15549.

[18] Pham, T.; Forrest, K. A.; Nugent, P.; Belmabkhout, Y.; Luebke, R.; Eddaoudi, M.; Zaworotko, M. J.; Space, B. Understanding Hydrogen Sorption in a Metal–Organic Framework with Open-Metal Sites and Amide Functional Groups. *The Journal of Physical Chemistry C* **2013**, *117*, 9340–9354.

[19] Pham, T.; Forrest, K. A.; McLaughlin, K.; Tudor, B.; Nugent, P.; Hogan, A.; Mullen, A.; Cioce, C. R.; Zaworotko, M. J.; Space, B. Theoretical Investigations of CO_2 and H_2 Sorption in an Interpenetrated Square-Pillared Metal–Organic Material. *The Journal of Physical Chemistry C* **2013**, *117*, 9970–9982.

[20] Forrest, K. A.; Pham, T.; Hogan, A.; McLaughlin, K.; Tudor, B.; Nugent, P.; Burd, S. D.; Mullen, A.; Cioce, C. R.; Wojtas, L.; Zaworotko, M. J.; Space, B. Computational Studies of CO_2 Sorption and Separation in an Ultramicroporous Metal–Organic Material. *The Journal of Physical Chemistry C* **2013**, *117*, 17687–17698.

[21] Forrest, K. A.; Pham, T.; Nugent, P.; Burd, S. D.; Mullen, A.; Wojtas, L.; Zaworotko, M. J.; Space, B. Examining the Effects of Different Ring Configurations and Equatorial Fluorine Atom Positions on CO_2 Sorption in [Cu(bpy)$_2$SiF$_6$]. *Crystal Growth & Design* **2013**, *13*, 4542–4548.

[22] Pham, T.; Forrest, K. A.; Hogan, A.; McLaughlin, K.; Belof, J. L.; Eckert, J.; Space, B. Simulations of Hydrogen Sorption in *rht*-MOF-1: Identifying the Binding Sites Through Explicit Polarization and Quantum Rotation Calculations. *Journal of Materials Chemistry A* **2014**, *2*, 2088–2100.

[23] Pham, T.; Forrest, K. A.; Eckert, J.; Georgiev, P. A.; Mullen, A.; Luebke, R.; Cairns, A. J.; Belmabkhout, Y.; Eubank, J. F.; McLaughlin, K.; Lohstroh, W.; Eddaoudi, M.; Space, B. Investigating the Gas Sorption Mechanism in an *rht*-Metal–Organic Framework through Computational Studies. *The Journal of Physical Chemistry C* **2014**, *118*, 439–456.

[24] van Duijnen, P. T.; Swart, M. Molecular and Atomic Polarizabilities: Thole's Model Revisited. *The Journal of Physical Chemistry A* **1998**, *102*, 2399–2407.

[25] Applequist, J.; Carl, J. R.; Fung, K.-K. Atom dipole interaction model for molecular polarizability. Application to polyatomic molecules and determination of atom polarizabilities. *Journal of the American Chemical Society* **1972**, *94*, 2952–2960.

[26] Thole, B. Molecular polarizabilities calculated with a modified dipole interaction. *Chemical Physics* **1981**, *59*, 341 – 350.

[27] Bode, K. A.; Applequist, J. A New Optimization of Atom Polarizabilities in Halomethanes, Aldehydes, Ketones, and Amides by Way of the Atom Dipole Interaction Model. *The Journal of Physical Chemistry* **1996**, *100*, 17820–17824.

[28] Wolf, D.; Keblinski, P.; Phillpot, S. R.; Eggebrecht, J. Exact method for the simulation of Coulombic systems by spherically truncated, pairwise r^{-1} summation. *Journal of Chemical Physics* **1999**, *110*, 8254.

[29] Fennell, C. J.; Gezelter, J. D. Is the Ewald summation still necessary? Pairwise alternatives to the accepted standard for long-range

electrostatics. *Journal of Chemical Physics* **2006**, *124*, 234104.

[30] McLaughlin, K.; Cioce, C. R.; Pham, T.; Belof, J. L.; Space, B. Efficient calculation of many-body induced electrostatics in molecular systems. *Journal of Chemical Physics* **2013**, *139*, 184112.

[31] Belof, J. L. Theory and simulation of metal–organic materials and biomolecules. Ph.D. thesis, University of South Florida, 2009.

[32] Dinh, T.-L.; Huber, G. A. An Efficient Algorithm for Polarizable Interactions: A Uniformly Distributed One-Dimensional Case. *Journal of Mathematical Modelling and Algorithms* **2005**, *4*, 111–128.

[33] Palmo, K.; Krimm, S. Theoretical basis and accuracy of a non-iterative polarization protocol in molecular mechanics energy function calculations. *Chemical Physics Letters* **2004**, *395*, 133–137.

[34] Metropolis, N.; Rosenbluth, A. W.; Rosenbluth, M. N.; Teller, A. H.; Teller, E. Equation of state calculations by fast computing machines. *Physics Letters B* **1953**, *21*, 1087–1092.

[35] McQuarrie, D. A. *Statistical Mechanics*; University Science Books: Sausalito, CA, 2000; Chapt. 3, pg. 53.

[36] Frenkel, D.; Smit, B. *Understanding Molecular Simulation: From Algorithms to Applications*; Academic Press: New York, 2002; Chapt. 5, Sect. 6.1, p.129.

[37] Boublík, T. The BACK equation of state for hydrogen and related compounds. *Fluid Phase Equilibria* **2005**, *240*, 96–100.

[38] Peng, D.-Y.; Robinson, D. B. A New Two-Constant Equation of State. *Industrial and Engineering Chemistry Fundamentals* **1976**, *15*, 59–64.

[39] Ewald, P. P. Die Berechnung optischer und elektrostatischer Gitterpotentiale. *Annalen der Physik* **1921**, *369*, 253–287.

[40] Feynman, R. P.; Hibbs, A. R. *Quantum Mechanics and Path Integrals*; McGraw-Hill: New York, 1965; Chapt. 10, Sect. 3, pg. 281.

[41] Siperstein, F.; Myers, A.; Talu, O. Long range corrections for computer simulations of adsorption. *Molecular Physics* **2002**, *100*, 2025–2030.

[42] Myers, A. L.; Monson, P. A. Adsorption in Porous Materials at High Pressure: Theory and Experiment. *Langmuir* **2002**, *18*, 10261–10273.

[43] Lässig, D.; Lincke, J.; Moellmer, J.; Reichenbach, C.; Moeller, A.; Gläser, R.; Kalies, G.; Cychosz, K. A.; Thommes, M.; Staudt, R.; Krautscheid, H. A Microporous Copper Metal–Organic Framework with High H_2 and CO_2 Adsorption Capacity at Ambient Pressure. *Angewandte Chemie International Edition* **2011**, *50*, 10344–10348.

[44] Nicholson, D.; Parsonage, N. G. *Computer Simulation and the Statistical Mechanics of Adsorption*; Academic Press: London, 1982.

[45] Belof, J. L.; Space, B. Massively Parallel Monte Carlo (MPMC). Available on Google Code, 2012.

[46] Talu, O.; Myers, A. L. Molecular Simulation of Adsorption: Gibbs Dividing Surface and Comparison with Experiment. *AIChE Journal* **2001**, *47*, 1160 – 1168.

[47] Garberoglio, G.; Skoulidas, A. I.; Johnson, J. K. Adsorption of Gases in Metal Organic Materials: Comparison of Simulations and Experiments. *The Journal of Physical Chemistry B* **2005**, *109*, 13094–13103, PMID: 16852629.

[48] Belof, J. L.; Stern, A. C.; Space, B. An Accurate and Transferable Intermolecular Diatomic Hydrogen Potential for Condensed Phase Simulation. *Journal of Chemical Theory and Computation* **2008**, *4*, 1332–1337.

[49] Mullen, A. L.; Pham, T.; Forrest, K. A.; Cioce, C. R.; McLaughlin, K.; Space, B. A Polarizable and Transferable PHAST CO_2 Potential for Materials Simulation. *Journal of Chemical Theory and Computation* **2013**, *9*, 5421–5429.

[50] Plimpton, S. Fast parallel algorithms for short-range molecular dynamics. *Journal of Computational Physics* **1995**, *117*, 1–19.

[51] Hogan, A.; Space, B. LAMMPS Induced-Dipole Polarization Pair Style. Available on Google Code, 2013.